The "Shadow Effect" in Colloid Transport and Deposition Dynamics in Granular Porous Media: Measurements and Mechanisms

ARTICLE *in* ENVIRONMENTAL SCIENCE AND TECHNOLOGY · AUGUST 2000

Impact Factor: 5.33 · DOI: 10.1021/es0009323

2 AUTHORS, INCLUDING:

Menachem Elimelech
Yale University
395 PUBLICATIONS **32,645** CITATIONS

Environ. Sci. Technol. **2000**, *34,* 3681−3689

The "Shadow Effect" in Colloid Transport and Deposition Dynamics in Granular Porous Media: Measurements and Mechanisms

CHUN-HAN KO AND
MENACHEM ELIMELECH*
Department of Chemical Engineering, Environmental Engineering Program, Yale University, P.O. Box 208286, New Haven, Connecticut 06520-8286

The role of hydrodynamic and colloidal interactions in the transport and deposition dynamics of colloidal particles in granular porous media is systematically investigated. Colloid transport experiments were conducted with three suspensions of positively charged colloidal latex particles (133, 288, and 899 nm in diameter) and negatively charged packed quartz grains. The column experiments were carried out under a wide range of solution ionic strengths ($10^{-5.5}$—$10^{-2.0}$ M) and approach velocities ($10^{-4.5}$—$10^{-2.5}$ m/s) until a complete breakthrough was attained, thus allowing unambiguous determination of the maximum attainable surface coverage for each deposition run. Results show that the rate of blocking and the maximum attainable surface coverage are determined by a unique interplay between flow intensity, particle size, and solution ionic strength. It is suggested that the tangential or shear component of the fluid flow around collector grains creates a "shadow zone" on the collector surface down gradient of deposited particles where the probability of subsequent deposition is substantially reduced. The shadow zone is determined by the combined effect of hydrodynamic interaction and electrostatic double layer repulsion. Increasing the approach velocity and particle size and decreasing the solution ionic strength result in a larger area of the shadow zone and hence reduced maximum attainable surface coverages. It is also proposed that sand grain surface roughness influences the dynamics of particle deposition by creating shadow zones down gradient of surface protrusions where particle deposition is significantly hindered.

Introduction

The dynamics of colloid transport and deposition in granular porous media are important in a variety of environmental processes in natural and engineered aquatic systems. These processes include the transport of pathogenic microorganisms such as viruses and bacteria in groundwater (*1, 2*), deep bed (granular) filtration in water and wastewater treatment (*3*), and transport of colloidal contaminants in subsurface environments (*4, 5*). Of paramount importance in these processes is the accurate description of the time-dependent or transient rate of particle deposition onto the grains (collectors) comprising the granular porous media.

* Corresponding author phone: (203)432-2789; fax: (203)432-2881; e-mail: menachem.elimelech@yale.edu.

Colloid deposition onto mineral grain surfaces is a dynamic process characterized by transient or time-dependent deposition kinetics (*4, 7*−*9*). During the initial stage of deposition, while collector grain surfaces are still devoid of retained particles, a constant rate of particle deposition is observed. As colloidal particles accumulate on collector surfaces, the particle deposition process begins to exhibit transient behavior. The dynamic aspects of particle deposition have been experimentally observed as either an increasing or decreasing rate of deposition (*4, 8*−*10*). Whether the rate of colloid deposition rises or declines depends primarily on solution chemistry and the chemical characteristics of colloids and collector grains.

When colloid interaction forces are repulsive, a declining colloid deposition rate is generally observed. The decline in particle deposition rate is attributed to the reduced availability of deposition sites on collector grains as deposited particles exclude the immediate vicinity of the collector surface from subsequent deposition of particles. This surface exclusion phenomenon is termed *blocking* (*7, 8*). Under solution chemical composition giving rise to blocking, interparticle contact (attachment) is prohibited so that the maximum density of retained particles on collector grain surfaces is a monolayer. The fractional surface coverage of collector grains in a completed monolayer is an important parameter and is referred to as the *maximum attainable surface coverage* or the *jamming limit* (*7, 8, 11*). Alternatively, the extent of blocking can be quantified by the *excluded area parameter* which is the reciprocal value of the jamming limit. The excluded area parameter represents the ratio between the blocked area of collector grains and the projected area of deposited particles in a completed monolayer (*8, 9, 11*).

Previous studies of particle deposition dynamics have focused primarily on the effect of solution ionic strength on the rate and extent of surface coverage (*7, 8, 11*−*13*). Experimental investigations in model flow systems (*7, 12, 14, 15*) and granular porous media (*8, 11, 13, 16*) demonstrated an inverse relationship between the excluded area parameter and the logarithm of solution ionic strength, thus indicating that the area excluded or blocked by a deposited particle is largely determined by the thickness of the electrical double layer. Recent studies in stagnation point flow systems point out that flow intensity (*12, 17, 18*) or particle size (*18, 19*) influence the dynamics of particle deposition and the resulting maximum attainable surface coverage. These results may suggest that both hydrodynamic and colloidal interactions are important in the dynamics of particle deposition and blocking. None of these studies, however, provided a systematic investigation of the role of flow intensity or particle size on the dynamics of particle blocking. Moreover, the combined or coupled effect of hydrodynamic and colloidal interactions in flow through more complex and environmentally relevant geometries, such as granular porous media, has never been addressed.

The objective of this paper is to examine the interplay between hydrodynamic and double layer interactions and their effect on the dynamics of particle deposition and blocking during flow of colloidal particles through granular porous media. More specifically, the interplay between fluid flow rate, solution ionic strength, and particle size in controlling the extent of surface coverage and blocking is systematically investigated. Finally, the mechanisms governing the dynamics of blocking under the influence of hydrodynamic and double layer interactions are delineated and the so-called "shadow effect" is elucidated and discussed.

10.1021/es0009323 CCC: $19.00
Published on Web 08/04/2000

Materials and Methods

Colloidal Particles. Monodisperse suspensions of surfactant-free polystyrene latex particles with positively charged amidine surface functional groups (Interfacial Dynamics Corporation, Portland, OR) were used as model colloids in the deposition experiments. Three suspensions having mean particle diameters of 133, 288, and 899 nm and a density of 1.055 g/cm^3 were utilized. Particle diameters were determined by the manufacturer from measurement of 600 individual particles by transmission electron microscopy. The titrated surface charge densities of the 133, 288, and 899 nm particle suspensions (as given by the manufacturer) were 8.0, 15.5, and 22.3 μC/cm^2, respectively. Monodispersity of the colloidal suspensions was verified by dynamic light scattering measurements (Nicomp Model 370, Particle Sizing Systems, Santa Barbara, CA).

Granular Porous Media. Quartz sand was used as the column packing material (Aldrich Chemical, Milwaukee, WI). The sand was thoroughly cleaned prior to use. The cleaning procedure consisted of immersing the sand in sodium dithionite solution (0.1 M $Na_2S_2O_4$) for 2 h, soaking the sand in hydrogen peroxide (5% H_2O_2) for 3 h, and overnight soaking in hydrochloric acid (12 N HCl). Following each of these steps, the sand grains were thoroughly rinsed with deionized water.

Examination of the quartz sand with petrographic and scanning electron microscopy revealed the sand grains to be spherical in shape, with surfaces having a subangular to subrounded appearance. The quartz grains are well sorted, with a nominal grain diameter of 0.32 mm. The nominal grain diameter was determined by averaging the major and minor axes of 35 separate grains. Scanning electron micrographs of individual quartz grain surfaces revealed a significant degree surface roughness. The surfaces appear highly irregular, having sharp, angular terminations, jagged protrusions, and deep crevices.

To study the effect of the sand grain surface roughness on particle deposition dynamics, several sets of particle deposition experiments with spherical, uniform, and relatively smooth glass beads (Class V, Ferro Corp., Jackson, MS) were also carried out. The glass bead collectors had a mean diameter of 0.46 mm and chemical and physical properties as reported elsewhere (*11*). The glass beads were cleaned following the procedure described in Liu et al. (*11*).

Electrokinetic Characterization of Colloids and Granular Porous Media. Electrophoretic mobility measurements were used to determine the electrokinetic properties of the model latex particles and sand grains. The electrophoretic mobilities were measured using a Lazer Zee Model 501 apparatus (Pen Kem Inc., Bedford Hills, NY). To estimate the electrokinetic (zeta) potential of the sand grains, the electrophoretic mobility of colloidal-size fragments of the quartz sand grains were measured. The colloidal quartz suspensions were obtained by ultrasonication of clean sand grains in distilled water for 10 min. Electrokinetic potentials of the glass beads as a function of ionic strength were reported elsewhere (*11*).

Experimental Column Setup. Colloid transport experiments were conducted in a glass chromatography column packed with clean sand grains or glass beads. Adjustable-height glass columns (Omnifit USA, Toms River, NJ) with either 10 or 17 mm inner diameter were used. Columns had a 125 μm polyethylene wire mesh on both ends. The columns were wet-packed in a solution having the same chemical composition as the solution used during the subsequent column run. Column packing porosity for each experiment was determined as 0.37, based on a density of 2.59 g/cm^3 for sand and 2.45 g/cm^3 for glass beads.

A typical column experiment involved pumping an aqueous particle suspension through the packed column at a constant flow rate. To ensure smooth and accurate flow rate, high-performance liquid chromatography (HPLC) pumps (Accuflow series II, Fisher scientific, Pittsburgh, PA) were used. One HPLC pump was employed to deliver the colloid suspension, and a second HPLC pump was used to deliver an appropriate dosage of KCl solution at an identical flow rate as the first pump. The colloid suspension and KCl solution were mixed in-line just ahead of the column to avoid possible particle aggregation. Particle concentrations in the column effluent were monitored at 1−8 s intervals using optical density measurements with a UV/vis spectrophotometer (Hewlett-Packard Model 8452A) and a 1-cm flow-through cell.

Because the surface of the silica flow-through cell is negatively charged, positively charged amidine latex particles deposit on the inner cell surface and significantly influence the UV absorption reading. To avoid this problem, a third HPLC pump was used to deliver sodium dodecyl sulfate (SDS) aqueous solution to the column effluent right before the flow-through cell to reverse the charge of the amidine latex particles (from positive to negative) and thus prevent their attachment to the negatively charged flow through cell surface. The final concentration of SDS in the colloidal suspension in the flow through cell was 5×10^{-4} M. The procedure was verified in separate preliminary experiments of latex particle calibrations in the presence of 5×10^{-4} M SDS.

Colloid Deposition Dynamics Experiments. To determine experimentally the maximum attainable surface coverage under the various physical and chemical conditions, each colloid deposition experiment was proceeded until a complete breakthrough was attained (i.e. $C/C_0 = 1.0$). The initial colloid concentrations used were 30 mg/L for the 133 and 288 nm particles and 80 mg/L for the 899 nm particles (or 2.31×10^{10}, 2.27×10^9, and 1.99×10^8 cm^{-3} for the 133, 288, and 899 nm particles, respectively). Columns were packed to a depth ranging from 1.0 to 15.5 cm, depending on the particle size and approach velocity for the corresponding run. Prior to the introduction of suspended colloids to the column, a colloid-free solution with a chemical composition similar to that of the subsequent deposition experiment was delivered to the column for at least 30 min. The colloid suspension was then introduced to the packed column for periods ranging from about 1 to 30 h (or up to over 1000 pore volumes), depending on the physical and chemical conditions of the specific run, until a complete breakthrough was reached. Following the deposition run, a colloid-free solution having the same chemical composition as that used during the deposition stage was introduced to obtain the elution curve.

The first set of experiments was designed to determine the excluded area parameter (or maximum attainable surface coverage) of the model colloidal particles and sand grains over a wide range of ionic strengths. Experiments were performed at various ionic strengths corresponding to the half-log intervals spanning the range of DI water (ionic strength $10^{-5.5}$) up to 10^{-2} M. For each particle size, column experiments over the above ionic strength range were conducted at approach velocities of 10^{-3} and 10^{-4} m/s.

The second set of experiments investigated the effect of particle size and flow velocity. For each of the three particle suspensions, experiments were performed at various flow (approach) velocities corresponding to the half-log intervals within the range of $10^{-4.5}$–$10^{-2.5}$ m/s, at a constant ionic strength of 10^{-4} M KCl. To investigate the effect of surface roughness, column experiments over the above physicochemical conditions were conducted using both sand and glass beads as granular porous media.

The third set of experiments was designed to further elucidate the so-called shadow effect by demonstrating that a higher flow velocity would create a larger "shadow zone"

TABLE 1. Electrokinetic (Zeta) Potentials of Colloidal Particles and Sand Grains as a Function of Ionic Strength

	electrokinetic (zeta) potential (mV)			
ionic strength (M)	133 nm	288 nm	899 nm	quartz sand
DI water[a]	71	68	58	−75
$10^{-5.25}$	77	76	59	−65
$10^{-5.0}$	79	72	59	−65
$10^{-4.5}$	69	51	48	−56
$10^{-4.0}$	61	47	39	−51
$10^{-3.5}$	47	41	34	−39
$10^{-3.0}$	41	36	29	−34
$10^{-2.5}$	27	31	24	−24
$10^{-2.0}$	21	27	18	−16

[a] Deionized water has an ionic strength $\approx 10^{-5.5}$ M, based on electrical conductivity measurements.

and correspondingly a larger excluded area. A 30 mg/L suspension of 288 nm particles at an ionic strength of 10^{-4} M KCl was delivered to an 8-cm column at a constant fluid approach velocity of 10^{-3} m/s until a complete breakthrough was attained. A particle-free solution at an identical flow rate and chemical composition was followed for 20 more pore volumes to dislodge any undeposited interstitial colloids. At the end of this step, the approach velocity was reduced to 10^{-4} m/s, and the same concentration of 288 nm particles was delivered until a complete breakthrough was attained. In this last deposition stage (at 10^{-4} m/s), the column length and ionic strength were the same as in the first stage (i.e., 8 cm and 10^{-4} M KCl).

Room temperature was maintained during all column runs (about 21 °C). Solution pH of influent and effluent showed little or no variation during the experiments, remaining between 5.6 and 5.8. All column apparatus and accessories were carefully cleaned between experimental runs with a strong acid (HCl) and deionized water.

Results and Discussion

Electrokinetic Potentials of Colloidal Particles and Sand Grains. The electrokinetic (zeta) potentials of the particles and sand grain colloidal fragments were calculated from the measured electrophoretic mobilities using the tabulated values of Ottewill and Shaw (*20*) which have been corrected for relaxation and retardation effects. Table 1 presents the zeta potentials of the colloidal particles and quartz grains as a function of electrolyte (KCl) concentration. For both particles and sand grains, the absolute value of the zeta potential decreases with increasing ionic strength due to double layer compression and reduction of the Stern potential. Particles and collectors bear opposite surface charge thus allowing the blocking effect to be examined under "favorable", irreversible particle deposition conditions during the column experiments.

Colloid Breakthrough Curves. Typical colloid breakthrough curves illustrating the effect of ionic strength on colloid transport and deposition behavior are shown in Figure 1. The data are displayed as normalized effluent particle concentration (C/C_0) as a function of pore volume, with the latter being defined as the product of time and approach velocity divided by the product of column length and porosity. Contrary to previous colloid deposition dynamics studies (*8, 13, 16*), all colloid breakthrough runs are carried out until C/C_0 approaches unity, thus allowing unambiguous determination of the maximum attainable surface coverage. After the initial breakthrough (at about 1 pore volume), which corresponds to the initial deposition rate (or the so-called "clean bed" removal), the residual particle concentration in the column effluent increases due to reduction in colloid deposition rate associated with blocking (excluded area) effects (*8, 11, 13, 16*). Solution ionic strength has a marked

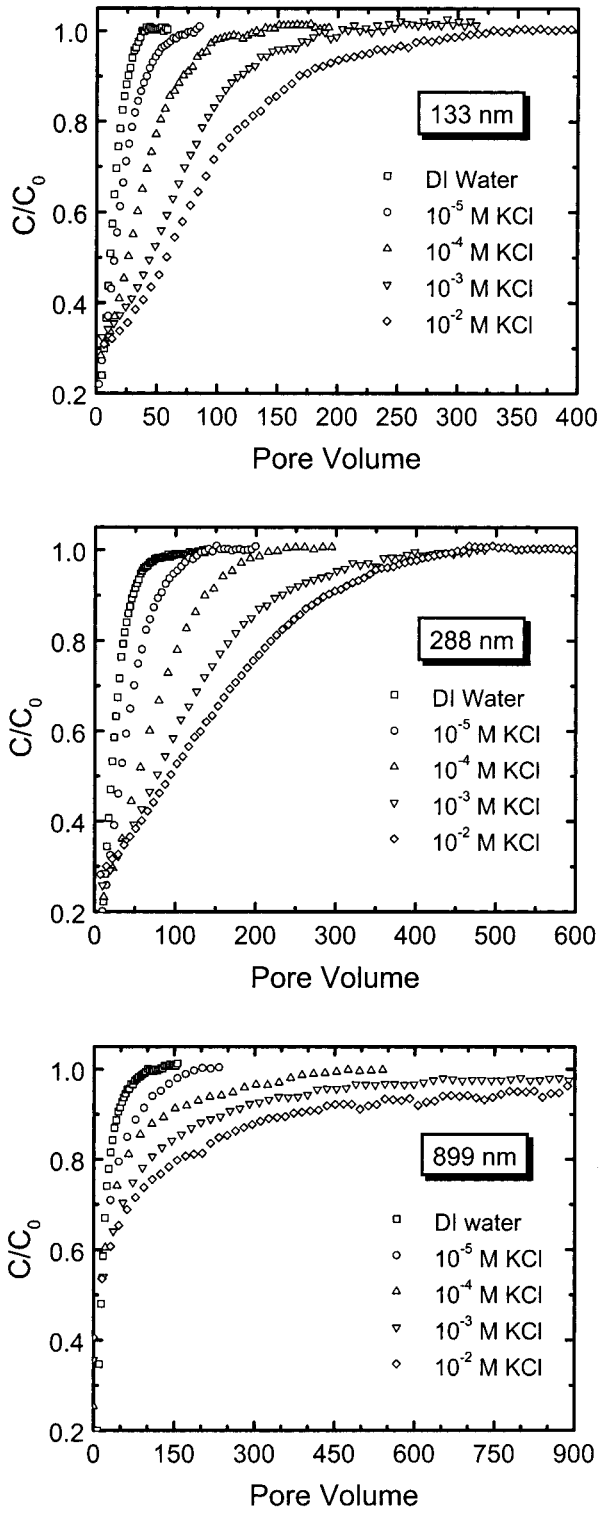

FIGURE 1. Particle breakthrough curves for the three colloidal suspensions illustrating the influence of solution ionic strength on the colloid transport and deposition dynamics. Column experiments were carried out at an approach velocity of 10^{-4} m/s, solution pH of 5.7, and temperature of 21 °C. Other experimental conditions were as follows: sand grain diameter was 0.32 mm; particle concentrations for the 133, 288, and 899 nm particle column runs were 30, 30, and 80 mg/L (2.31×10^{10}, 2.27×10^{9}, and 1.99×10^{8} cm^{-3}), respectively; column lengths for the 133, 288, and 899 nm particle runs were 1.0, 2.0, and 2.5 cm, respectively. Note that the solution ionic strength of deionized water (DI) is ca. $10^{-5.5}$ M.

effect on colloid deposition dynamics. At lower ionic strengths, breakthrough curves are steeper and C/C_0 ap-

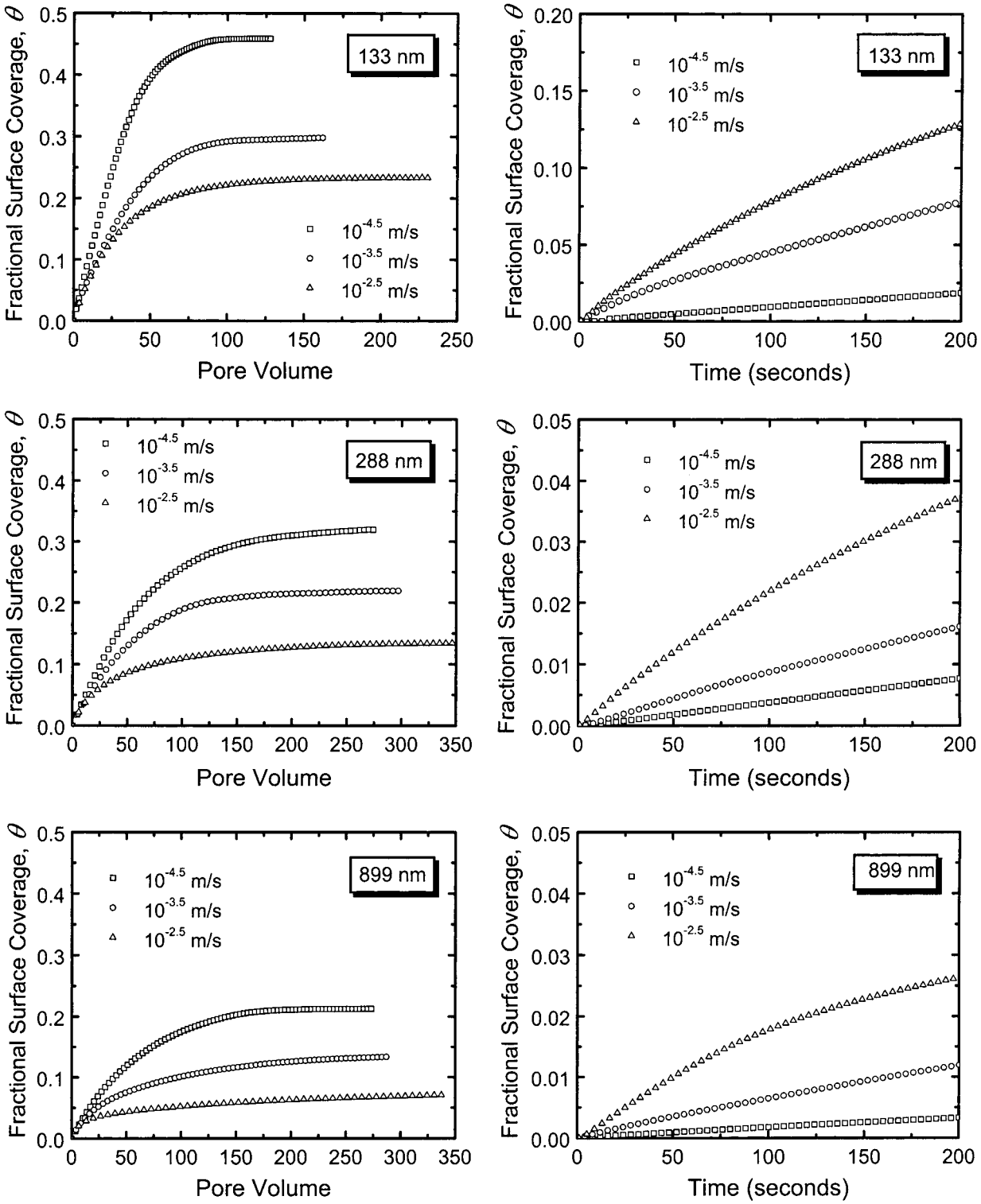

FIGURE 2. The evolution of fractional surface coverage of sand grains with time for the three colloidal suspensions as determined from a set of column experiments at various approach velocities. The figures on the left depict the change of θ with pore volume for the entire colloid transport run (*i.e.,* until a complete breakthrough is attained). The figures on the right depict the change of θ with time for the initial stages of deposition. Experiments were carried out at a fixed ionic strength of 10^{-4} M, solution pH of 5.7, and temperature of 21 °C. Other experimental conditions are described in Materials and Methods.

proaches unity much faster than at higher ionic strengths. For a given particle size, the rate of approach to total breakthrough ($C/C_0 = 1$) is an indication of the relative area blocked by a deposited particle, with steeper breakthrough curves corresponding to larger excluded areas (*8, 11, 16*).

Dynamics of Surface Coverage. The dynamics of particle deposition in granular porous media and the blocking phenomenon are best illustrated as the changing rate at which collector surfaces are covered by deposited particles. The fractional collector surface coverage θ can be obtained as a function of time from the experimental particle breakthrough data using (*11*)

$$\theta = \frac{\pi a_p^2 U a_c C_0 \int_0^t (1 - C/C_0)\mathrm{d}t}{3L(1-\epsilon)} \quad (1)$$

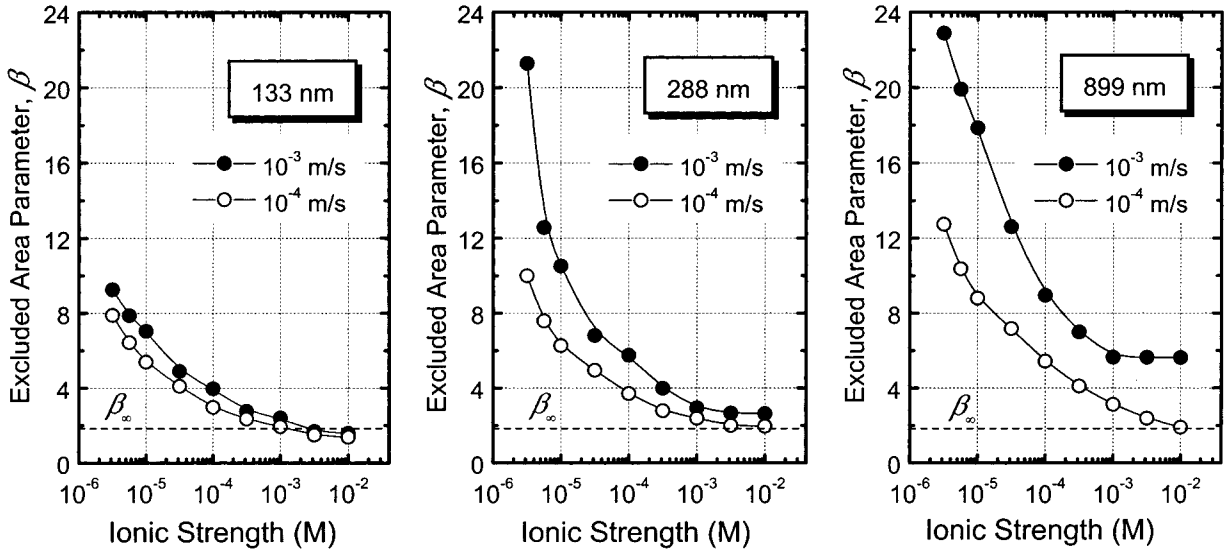

FIGURE 3. The change of excluded area parameter ($\beta = 1/\theta_{max}$) with solution ionic strength for the three colloidal suspensions as determined from column experiments at two different approach velocities (10^{-3} m/s for top curves and 10^{-4} m/s for bottom curves). Values of θ_{max} were determined from particle breakthrough curves that attained a complete breakthrough. For instance, the θ_{max} values at 10^{-4} m/s (open circles) were determined from the breakthrough curves shown in Figure 1. Other experimental conditions are described in Materials and Methods. The bottom dashed horizontal line in each figure, labeled as β_∞ (= 1.83), corresponds to the hard sphere jamming limit, $\theta_\infty = 0.546$.

Here a_p is the particle radius, a_c is the collector radius, U is the fluid approach (superficial) velocity, C_0 is the column inlet particle number concentration, C is the column effluent particle number concentration corresponding to time t, L is the packed bed column length, and ϵ is the bed porosity.

An illustration of the dynamic nature of fractional surface coverage for column transport experiments at approach velocities ranging from $10^{-4.5}$ to $10^{-2.5}$ m/s and a fixed ionic strength of 10^{-4} M KCl is given in Figure 2. The declining slopes associated with fractional surface coverage are indicative of the transient particle deposition rate resulting from blocking of collector surfaces. As particle deposition proceeds toward completion of a monolayer, blocking produces a declining fractional surface coverage rate that eventually reaches zero at the maximum attainable surface coverage (jamming limit). The slope of the curves at very short deposition times before blocking becomes significant (Figure 2 right side) is directly related to the initial particle deposition rate. A comparison of the surface coverage curves versus pore volume (Figure 2 left side) reveals that blocking is more pronounced for larger particles and higher flow rates. Higher flow rates and larger particles result in maximum attainable surface coverage values that are considerably less than the values associated with the smaller particles and lower flow rates. This important effect of particle size and flow rate is related to the so-called shadow effect that will be elucidated and discussed in detail later in this paper.

Dependence of Excluded Area on Solution Ionic Strength. The collector surface area blocked by deposited particles in a completed monolayer is inversely proportional to the maximum attainable surface coverage θ_{max}. The excluded area parameter β defines the dimensionless ratio of blocked collector surface area to the projected area of particles in a completed monolayer and is determined as the reciprocal value of θ_{max}:

$$\beta = \frac{1}{\theta_{max}} \tag{2}$$

The dependence of the excluded area on solution ionic strength for the three colloidal suspensions is depicted in Figure 3. For each particle suspension, results are shown for two approach velocities: 10^{-3} and 10^{-4} m/s. Inspection of the excluded area curves reveal three distinct features. First, the excluded area decreases as the solution ionic strength is increased. Second, larger excluded areas are associated with larger particles. Last, the excluded area is influenced by the approach velocity, with larger β values associated with higher approach velocities.

The excluded area parameter exhibits an inverse logarithmic dependence on electrolyte concentration (or ionic strength). The decline in β corresponds to "hardening" of particles as increasing electrolyte concentration compresses the diffuse double layer surrounding the particles. Rather large excluded areas are associated with deionized water (ionic strength ca. 6×10^{-6} M), especially for the larger particles where β is in excess of 20. It is striking that in a solution ionic strength of 6×10^{-6} M (deionized water), deposition of the 288 and 899 nm particles produces a completed monolayer (i.e., full blocking of collector surface) at fractional surface coverages of only 4.7% and 4.4%, respectively.

Under conditions of irreversible monolayer particle deposition, random sequential adsorption (RSA) modeling predicts that the lowest value that the excluded area parameter may attain is 1.83—the reciprocal of the "hard sphere" jamming limit value of 0.546 (*7, 8, 21*). The experimental results show that the excluded area values approach the asymptotic limit of $\beta_\infty = 1.83$ (shown as a dashed horizontal line) at high ionic strengths. The values of β below 1.83 noted in Figure 3 may be attributable to deviation from monolayer coverage of collector surfaces at high ionic strengths due to reduced colloidal stability which result in multilayer deposition.

Influence of Flow Intensity on the Maximum Attainable Surface Coverage. The previous results show that, in addition to solution ionic strength, the excluded area is influenced by the approach velocity in the packed bed. A more systematic investigation of the effect of flow velocity is shown in Figure 4, where the variation of the maximum attainable surface coverage θ_{max} with approach velocity at a fixed ionic strength of 10^{-4} M is displayed for the three colloidal suspensions. The maximum attainable surface coverage decreases substantially with increasing approach velocity. Furthermore, much smaller θ_{max} values are obtained for larger colloidal particles. Although the diffuse double layer thickness sur-

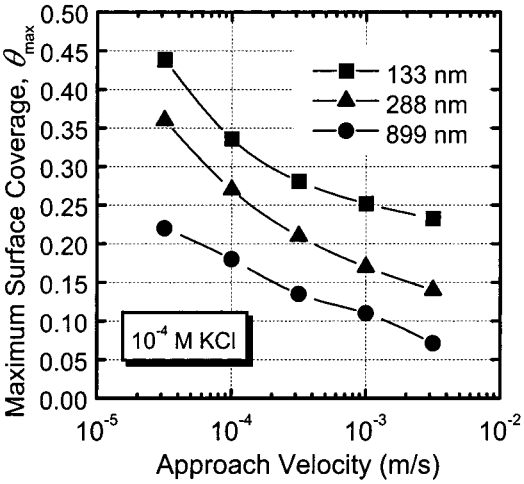

FIGURE 4. Maximum attainable surface coverage as a function of approach velocity for the three colloidal suspensions. Deposition experiments were carried out at a fixed solution ionic strength of 10^{-4} M KCl. Other experimental conditions are described in Materials and Methods.

rounding the colloidal particles is the same (30 nm at 10^{-4} M KCl) for all curves displayed in Figure 4, the smaller particles (133 nm) attain a θ_{max} value as high as 44% at the lowest approach velocity (3.16×10^{-5} m/s), whereas the largest particles (899 nm) attain a θ_{max} value of only 7% at the highest approach velocity (3×10^{-3} m/s). This rather unique dependence of the maximum attainable surface coverage on flow velocity and particle size is attributed to the shadow effect which is elucidated in the following subsection. One should also note that the observed results of larger θ_{max} values for smaller particles at the given low ionic strength of 10^{-4} M are in contrast with theoretical predictions and experimental observations which suggest a decrease in θ_{max} as particle size decreases when only electrostatic double layer interaction is considered (*18, 19*). The observed "anomalous" behavior in Figure 4 with respect to particle size is again attributed to the shadow effect which cannot be ignored for the physicochemical conditions prevailing in our colloid transport experiments.

Interplay Among Flow Intensity, Particle Size, and Ionic Strength: The Shadow Effect. The results discussed so far demonstrated that the rate of blocking as well as the excluded area parameter β increase with decreasing solution ionic strength and increasing particle size and approach velocity. The excluded area (or the maximum attainable surface coverage) is determined by a unique interplay between colloidal (mostly electric double layer) and hydrodynamic interactions. These interactions for particle deposition from flowing suspensions, as in packed beds, are controlled by flow intensity, particle size, and solution ionic strength (*7, 8, 17*). Their combined effect on the blocking rate and the excluded area is explained by the so-called shadow effect which is described schematically in Figure 5.

The flow around a spherical collector has both tangent and radial components. The tangential or shear component of the fluid flow creates a shadow zone on the collector surface down gradient of a deposited particle where the probability of subsequent deposition is reduced by the combined effect of hydrodynamic interaction and electrostatic double layer repulsion (*8, 17*). For a given ionic strength, the size of this excluded region increases as the particle size and the approach velocity increase. Smaller particles and lower approach velocities result in more efficient diffusive transport and, hence, a smaller shadow region. The shadow region is also influenced by solution ionic strength due to electrostatic double layer repulsion between deposited and approaching

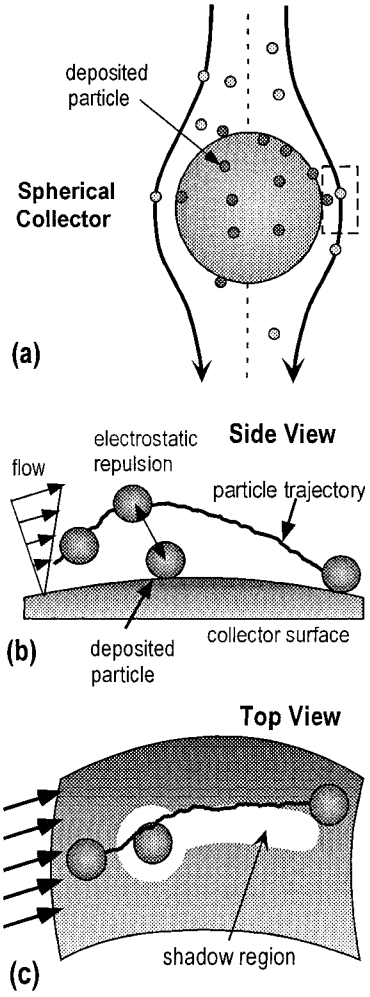

FIGURE 5. Schematic description of the shadow effect where the interplay among particle size, approach velocity, and solution ionic strength controls the maximum attainable surface coverage and the dynamics of deposition onto a spherical collector. (a) Flow around a spherical collector with the dashed axis line passing through the forward (top hemisphere) and rear (bottom hemisphere) stagnation points. (b) Side view of the region enclosed by the dashed box in the figure above, where the tangent flow and the resulting shadow effect are maximal at an angle of 90 degrees from the forward stagnation point. (c) Shadow region downgradient of a deposited particle and the resulting increase in the excluded area due to the coupling between hydrodynamic and colloidal interactions.

particles, with lower ionic strengths resulting in an extended shadow zone for a given particle size and approach velocity.

On a spherical collector surface, the tangent flow and the fluid shear depend on the location on the collector surface with respect to the stagnation point (*8*), thus resulting in a position-dependent value for the excluded area parameter. The forward and rear stagnation points are the only locations on a spherical collector not subject to the shadow effect, whereas the region midway between the stagnation points will experience the largest shadow zone. Because of the dependence of the excluded area parameter on angular position along a spherical collector, experimentally determined β values represent a spatial average of the entire collector surface, thus further complicating any theoretical analysis of this complex phenomenon.

To assess the importance of hydrodynamic interactions on particle deposition dynamics and the maximum attainable surface coverage, a particle Peclet number is defined in terms of the interstitial velocity v_p (i.e., approach velocity divided by porosity) and the particle radius a:

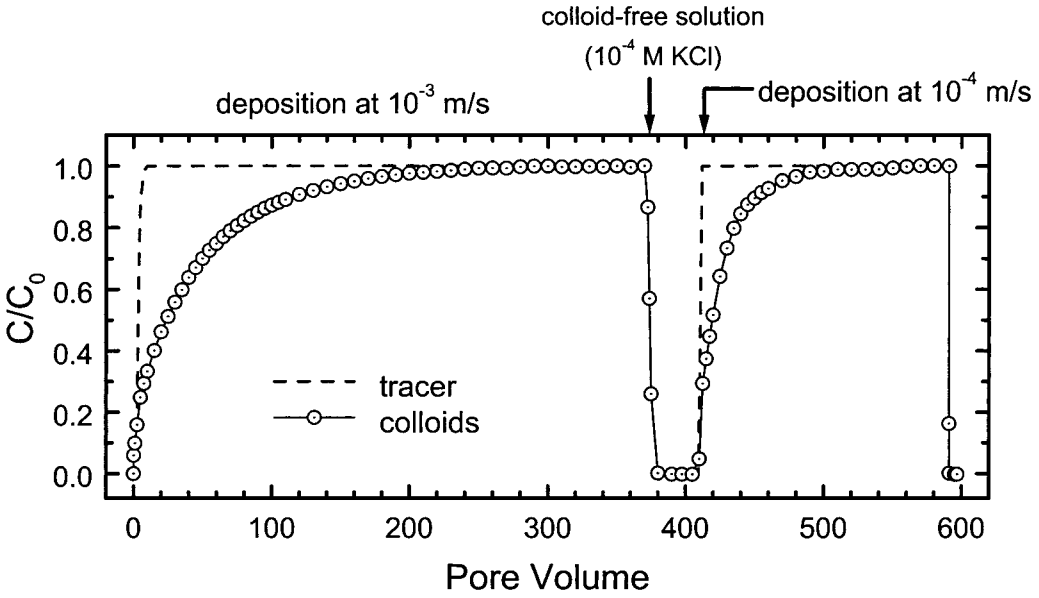

FIGURE 6. Illustration of the unique dependence of the shadow zone and the resulting surface coverage on the approach velocity during deposition of the 288 nm particles in the quartz grain packed columns. The column deposition experiment at the first stage was carried out at an approach velocity of 10^{-3} m/s, whereas the deposition run at the second stage was carried out at 10^{-4} m/s. The solution ionic strength in the experiments was fixed at 10^{-4} M KCl. A particle-free solution (10^{-4} M KCl) was used between the two particle deposition stages. Column length for the experiments in both stages was 8 cm. Other experimental conditions are described in Materials and Methods.

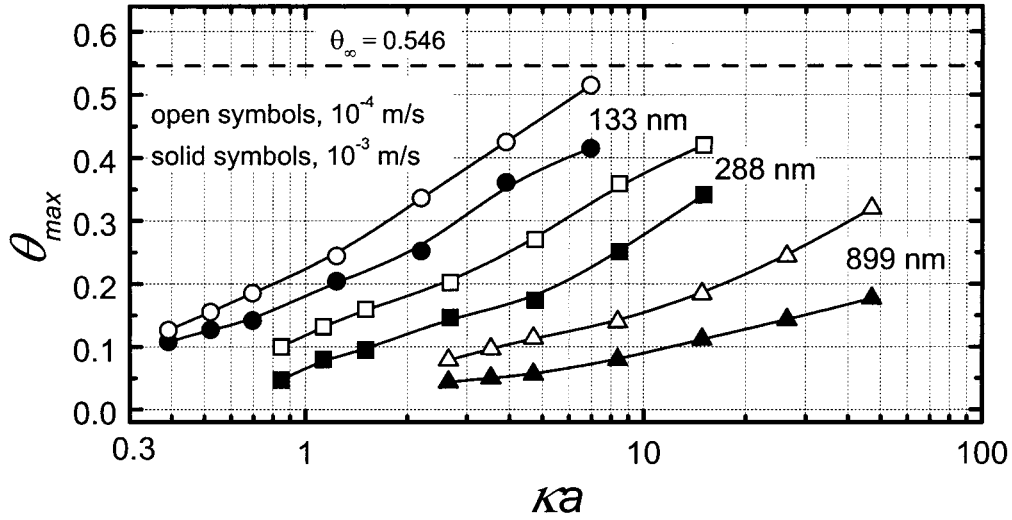

FIGURE 7. Dependence of the maximum attainable surface coverage (θ_{max}) on the electrostatic double layer interaction parameter (κa) for the three particle suspensions (133, 288, and 899 nm) at two approach velocities, 10^{-4} m/s (open symbols) and 10^{-3} m/s (solid symbols). Data for θ_{max} were obtained from Figure 3 for ionic strengths where monolayer deposition prevails (i.e., ionic strength smaller or equal to 10^{-3} M). The dashed line at the top corresponds to the hard sphere jamming limit, $\theta_\infty = 0.546$.

$$Pe = \frac{v_p a}{D_\infty} = \frac{6\pi\mu v_p a^2}{kT} \qquad (3)$$

Here, μ is the solvent viscosity, D_∞ is the Stokes−Einstein particle diffusion coefficient, k is the Boltzmann constant, and T is the absolute temperature. It is expected that hydrodynamic interactions become important when the Peclet number is greater than ca. 1. Hydrodynamic interactions will not influence the maximum attainable surface coverage only when $Pe \ll 1$. For all experimental conditions employed in this study, $Pe > 1$, attaining values greater than 2500 for the larger (899 nm) particles.

To further demonstrate the shadow effect and the important role of hydrodynamic interactions, the following column experiment depicted in Figure 6 was carried out. The 288 nm colloid suspension was delivered to the packed column at an approach velocity of 10^{-3} m/s and a solution ionic strength of 10^{-4} M until a complete breakthrough. This was followed by flushing the column with a particle-free solution having the same ionic strength (10^{-4} M) and at the same approach velocity for an additional 20 pore volumes. The colloid suspension was then reintroduced to the column at a much lower approach velocity (10^{-4} m/s), and particle deposition was continued until a complete breakthrough was attained. Using eq 1, the θ_{max} value for the first deposition stage at 10^{-3} m/s was calculated from the breakthrough curve to be 17.9%. If diffuse double layer thickness is the only factor determining the magnitude of θ_{max}, there should be no additional particle deposition for the same colloid suspension and ionic strength for the subsequent run at the lower approach velocity (10^{-4} m/s), because a complete monolayer of deposited particles was already achieved in the previous deposition stage. However, an additional 8.0% coverage was obtained in the subsequent deposition run at the lower

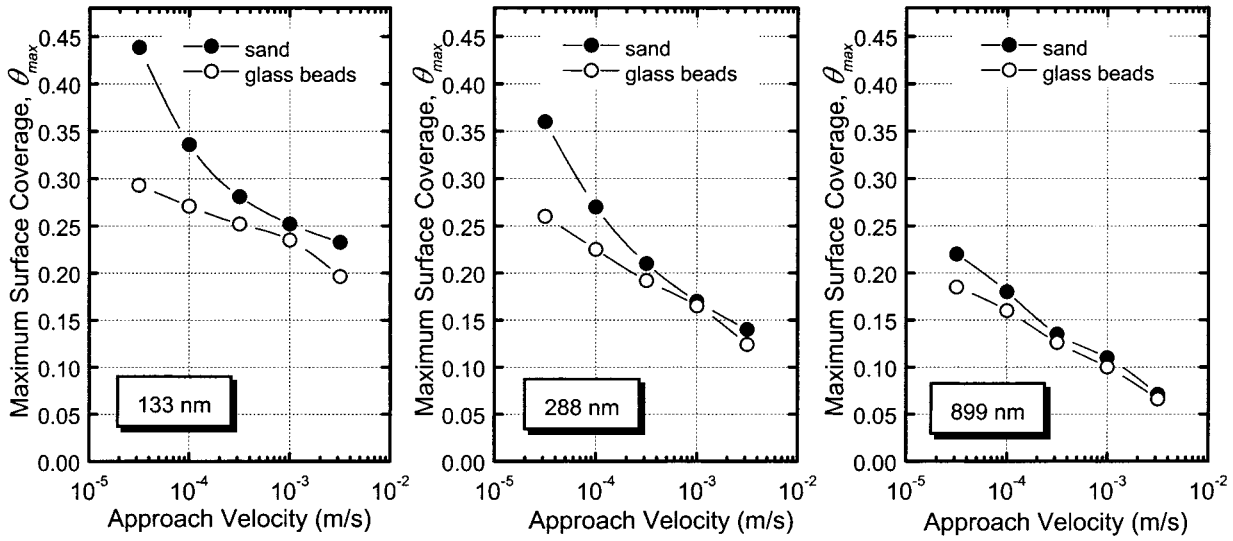

FIGURE 8. Comparison of the behavior of maximum attainable surface coverage versus approach velocity for particle deposition onto sand grains (top curves) or glass beads (bottom curves). The experiments with the three colloidal suspensions were carried out at a fixed ionic strength (10^{-4} M KCl). The difference in the behavior of the displayed curves is attributed to surface roughness of sand grains.

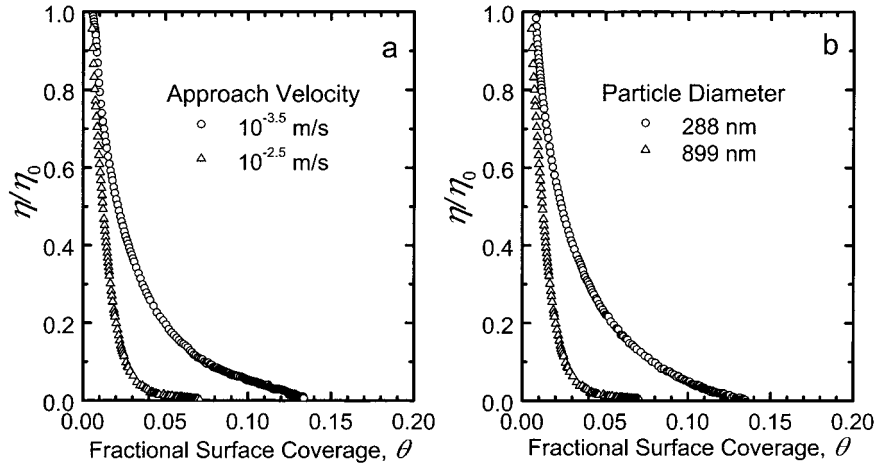

FIGURE 9. The nonlinear decline of particle deposition rate (expressed as normalized single collector efficiency, η/η_0) as a function of fractional surface coverage during particle deposition. The figure on the left (a) describes the deposition dynamic behavior of the 899 nm particles at two approach velocities and a solution ionic strength of 10^{-4} M KCl. The figure on the right (b) describes the deposition dynamics of the 288 and 899 nm particles at an approach velocity of $10^{-2.5}$ m/s and a solution ionic strength of 10^{-4} M KCl. The nonlinear behavior is largely attributed to the shadow effect.

approach velocity of 10^{-4} m/s. This observation clearly demonstrates the existence of a shadow region down gradient of deposited particles. Because of the shadow effect, there exists some surface area on the collectors that is not accessible to colloidal particles at the higher velocity of 10^{-3} m/s. This surface area, however, becomes accessible for deposition at the lower velocity of 10^{-4} m/s where the shadow effect is less significant. It should be noted that the cumulative θ_{max} of the two deposition stages (17.9% plus 8.0%) is remarkably close to the θ_{max} value of 27% independently obtained for the deposition run at 10^{-4} m/s described earlier in Figure 4.

Relative Role of Electrostatic and Hydrodynamic Interactions. Our previous results suggest that both hydrodynamic and electrostatic double layer interactions influence the maximum attainable surface coverage θ_{max}. It was clearly shown that lower ionic strengths are associated with lower θ_{max} due to longer range of repulsive double layer interactions. A useful dimensionless parameter characterizing the range of the electrostatic double layer interactions relative to the particle size is κa, where κ is the inverse Debye screening length and a is the particle radius. Under no flow conditions or in stagnation point flow systems where hydrodynamic interactions and the resulting shadow effect are absent, theoretical predictions and experimental results reveal a unique dependence of θ_{max} on κa (*15, 19*). Such results show that deposition of small colloidal particles of various sizes onto flat surfaces at different ionic strengths yields roughly similar θ_{max} versus κa curves, regardless of particle size. Plotting our previously shown dependence of excluded area on ionic strength (Figure 3) in this form, as depicted in Figure 7, results in remarkably different behavior. The results for the three particle suspensions (133, 288, and 899 nm) and two different approach velocities (10^{-4} and 10^{-3} m/s) clearly demonstrate that the θ_{max} versus κa curves are quite distinct and their slopes differ markedly. For a given κa, much smaller θ_{max} values are obtained for larger particles. Furthermore, as the particle size increases the slope of the θ_{max} versus κa curves decrease and the θ_{max} corresponding to the highest κa is much smaller than the hard sphere jamming limit ($\theta_\infty = 0.546$). This behavior signifies that hydrodynamic interactions control the θ_{max} behavior for the larger particles. The hydrodynamic conditions encountered in a granular porous medium are quite different from those prevalent in stagnation point flow systems or in quiescent fluids, and the flow field

dramatically modifies the deposition dynamics and the extent of surface coverage. The influence of hydrodynamic interactions is more pronounced for larger particles since a larger deposited particle will significantly modify the trajectory of an approaching particle of equal size. This is reflected in the generally very high values of the Peclet number (i.e., $Pe \gg 1$) for the larger particles as obtained from eq 3.

Effect of Collector Grain Surface Irregularities (Roughness). SEM images of the sand grains revealed significant surface roughness, with protrusions having dimensions much larger in scale than the particles used in the column experiments. To investigate the effect of the sand grain surface irregularities and roughness on θ_{max}, several sets of particle deposition experiments with uniform and relatively smooth glass beads were also carried out. A comparison of θ_{max} versus approach velocity curves for the glass beads and the sand grains at a fixed ionic strength of 10^{-4} M is shown in Figure 8. While the curves for the glass beads display a linear decrease in θ_{max} with an increase in the logarithm of the approach velocity, the corresponding curves for the sand grains show a clear nonlinear dependence at approach velocities smaller than 3×10^{-4} m/s for the 133 and 288 nm particles. It is postulated that a shadow region is created down gradient of large protrusions on the sand grains, somewhat analogous to that created by deposited particles. This shadow region is not accessible for particle deposition at high approach velocities or for large particles (899 nm). However, for smaller particles and at lower approach velocities, diffusive transport becomes important, and particle deposition down gradient of protrusions takes place, thus resulting in the nonlinear curves at low velocities. It is important to note that because the protrusions and particles are oppositely charged (i.e., there exists electrostatic attraction rather than repulsion as in the case with deposited particles), hydrodynamic interaction is the main cause for the shadow region downgradient of grain protrusions. Furthermore, it is worthwhile to emphasize that in our comparison of the θ_{max} curves we focused on the shape of the curves rather than the absolute value of θ_{max} since there may be some uncertainty in the absolute θ_{max} values for the sand grains as they were determined from eq 1 assuming that the surface area of the sand grains can be calculated from the grain mean diameter.

On the Nonlinear Dependence of Particle Deposition Rate on Surface Coverage. The nonlinear relationship between particle deposition rate and fractional surface coverage is the most salient feature of blocking dynamics by finite-size particles (*8*). Our previous work demonstrated that this nonlinearity is a direct result of excluded area effects exerted on collector surfaces by irreversibly deposited particles and is well predicted by the random sequential adsorption (RSA) model for particle blocking dynamics (*8*, *11*). Here we further demonstrate that this nonlinearity becomes more pronounced under conditions where the shadow effect is significant as illustrated in Figure 9. In this figure, the normalized single collector efficiency η/η_0 is depicted as a function of fractional surface coverage θ. The single collector efficiency η is obtained from the corresponding particle breakthrough curves as described elsewhere (*10*, *22*). The results are normalized with respect to the single collector efficiency corresponding to the initial stage of deposition, η_0. It is clearly shown that the nonlinearity in η/η_0 versus θ curves is much more pronounced for deposition at higher approach velocities (Figure 9a) and for larger particles (Figure 9b)—that is, for physicochemical conditions where the shadow effect is more pronounced. As demonstrated earlier in this paper, the shadow effect significantly magnifies the local value of the excluded area and the initial blocking rate by creating a shadow zone down gradient of deposited particles. For spherical collector grains, the size of the shadow zone varies with the angular position on the collector surface with respect to the stagnation point (*8*). This dependence of the shadow effect on angular position also produces nonuniform deposition on spherical collectors, which results in a nonlinear relation between deposition rate and fractional surface coverage (*8*, *23*).

Acknowledgments

The authors acknowledge the support of the National Science Foundation under Research Grant BES-9996240 (formerly BES 9705717).

Literature Cited

(1) Bales, R. C.; Hinkle, S. R.; Kroeger, T. W.; Stocking, K.; Gerba, C. P. *Environ. Sci. Technol.* **1991**, *25*, 2088−2095.
(2) Camesano, T. A.; Logan B. E. *Environ. Sci. Technol.* **1998**, *32*, 1699−1708.
(3) Tobiason, J. E.; O'Melia, C. R. *J. Am. Works Assoc.* **1998**, *80*, 54−64.
(4) Ryan, J. N.; Elimelech, M. *Colloids Surfaces A* **1996**, *107*, 1−56.
(5) McCarthy, J. F.; Zachara, J. M. *Environ. Sci. Technol.* **1989**, *23*, 496−502.
(6) Grolimund, D.; Borkovec, M.; Barmettler, K.; Sticher, H. *Environ. Sci. Technol.* **1996**, *30*, 3118−3123.
(7) Adamczyk, Z.; Siwek, B.; Zembala, M. Belouschek, P. *Adv. Colloid Interface Sci.* **1994**, *48*, 151−280.
(8) Johnson, P. R.; Elimelech, M. *Langmuir* **1995**, *11*, 801−812.
(9) Privman, V.; Frisch, H. L.; Ryde, N.; Matijevic, E. *J. Chem. Soc., Faraday Trans.* **1991**, *87*, 1371−1375.
(10) Elimelech, M.; O'Melia, C. R. *Environ. Sci. Technol.* **1990**, *24*, 1528−1536.
(11) Liu, D.; Johnson, P. R.; Elimelech, M., *Environ. Sci. Technol.* **1995**, *29*, 2963−2973.
(12) Adamczyk, Z.; Weronski, P. *Adv. Colloid Interface Sci.* **1999**, *83*, 137−226.
(13) Ryde, N.; Kihira H.; Matijevic, E. *J. Colloid Interface Sci.* **1992**, *151*, 421−432.
(14) Johnson, C. A.; Lenhoff, M. A. *J. Colloid Interface Sci.* **1996**, *179*, 587−599.
(15) Semmler M.; Mann E. K.; Ricka J.; Borkovec M. *Langmuir* **1998**, *14*, 5127−5132.
(16) Ryde, N.; Kallay, N.; Matijevic, E. *J. Chem. Soc., Faraday Trans.* **1991**, *87*, 1377−1381.
(17) Adamczyk, Z.; Siwek, B.; Szyk, L.; Zembala, M. *Bull. Pol. Acad. Sci. (Chem.)* **1993**, *41*, 41−54.
(18) Adamczyk, Z.; Siwek, B.; Zembala, M.; Weronski, P. *Langmuir* **1992**, *8*, 2605−2610.
(19) Bohmer, M. R.; van der Zeeuw, E. A.; Koper, G. J. M. *J. Colloid Interface Sci.* **1998**, *197*, 242−250.
(20) Ottewill, R. H.; Shaw, J. N. *J. Electroanal. Chem. Interfacial Electrochem.* **1972**, *37*, 133−142.
(21) Schaaf, P.; Talbot, J. *J. Chem. Phys.* **1989**, *91*, 4401−4409.
(22) Yao, K.-M.; Habibian, M. T.; O'Melia, C. R. *Environ. Sci. Technol.* **1971**, *5*, 1105−1112.
(23) Song, L.; Elimelech, M. *Colloids Surf. A* **1993**, *73*, 49−63.

Received for review January 24, 2000. Revised manuscript received June 14, 2000. Accepted June 22, 2000.

ES0009323